Natural Hazards (2021) 105:205–225
https://doi.org/10.1007/s11069-020-04305-0

ORIGINAL PAPER

A study on the motion and accumulation process of non-cohesive particles

Kunlin Lu[1] · **Yiming Chen**[1] · **Linfei Wang**[1]

Received: 4 December 2019 / Accepted: 31 August 2020 / Published online: 15 September 2020

Abstract
In order to further understand the mechanism of landslide-debris flow and predict the entire movement process and accumulation range of landslide hazards, the movement process of non-cohesive particles and the distribution of accumulation at the bottom of the slope were studied. Firstly, physical laboratory-scale tests on the sliding accumulation process of non-cohesive granular accumulations under self-weight were carried out, and the effects of different volumes and gradations on the sliding accumulation were analyzed. Then, the discrete element software PFC3D was used to perform three-dimensional numerical back analysis of the tests to refine the key parameters required for the numerical simulation, and to understand better the movement and accumulation state of the granular body. The results showed that the spherical particles exhibit obvious lateral expansion during the acceleration stage, and the front-end particles had a clear "shuttle" distribution, which became even more obvious with the increase in the content of large particles. The reverse-order phenomenon of spherical particles after sliding was that the proportion of small particles in the proximal end was far higher than their original proportion in the accumulation body. With the increase in the volume of the accumulation body, the phenomenon became more obvious, and stopping of large particles above the small particles was observed. The research results can provide reference for further studies of the movement process and the distribution patterns of the slip instability failures of non-cohesive accumulation bodies.

Keywords Landslide · Motion mechanism · Accumulation shape · Model experiment · Numerical simulation

1 Introduction

In recent years, China has experienced frequent strong earthquakes and extreme weather events, among which landslide geological disasters have had the highest frequency. The landslide-debris flow has an extremely high velocity and super-long migration distance. For example, in the landslide-debris flow that occurred in Yigong, Tibet, in 2000, the total volume of collapsed landslides exceeded 3.8×10^8 m^3, completely blocking the

✉ Kunlin Lu
lukunlin@hfut.edu.cn

[1] School of Civil Engineering, Hefei University of Technology, Hefei, Anhui, China

main stream of the Zangbu River and forming a barrier lake (Ren et al. 2001). In Wenjiagou, Sichuan Province, a large-scale landslide-debris flow occurred in the aftermath of the Wenchuan earthquake and a secondary geological disaster chain formed (Huang and Zhao 2010). In 2010, the area again experienced a large-scale debris-flow disaster (Ma and Wu 2011). In 2017, in Xinmocun, Maoxian, Fugui Mountain slid along the rock layer and disintegrated rapidly along the slope surface under the action of many factors, which characterizes the typical high-speed remote landslide-debris flow (Xu et al. 2011; He et al. 2017). Because landslide-debris flow can easily cause catastrophic accidents and result in significant loss of life and property, exploring the movement mechanisms of landslide-debris flows has become an important and popular research topic, both in China and worldwide.

The characteristics of high-speed and long-distance landslide-debris flow disasters, such as the sudden occurrence, complexity of movement and non-repeatability, make analyzing the geological disasters in situ difficult. Thus, model tests and numerical simulations need to be carried out to reflect the main features. Laboratory model tests and numerical simulations are important methods to verify the rationality of theoretical assumptions. Hutter and Koch (1991) designed a chute experimental device, using spherical glass beads and polystyrene particles as experimental materials, obtained the evolution curves of the front and rear edge velocities during landslide movement and discussed its evolution. Pudasaini et al. (2005) used dry sand as the test material, adopted an inclined-plate test device to obtain the velocity evolution characteristics of the debris flow along the inclined plate and compared them to the theoretical values to verify the correctness of the theoretical formulas. Manzella et al. (2008) designed an inclined-plate experimental device, discussed the influence of the slope angle of the source area, the particle size of the test material, and the instability volume on the movement characteristics of the debris flow and analyzed the energy loss occurring during sliding mass movement and accumulation, which provided some explanations for the long-distance characteristics of debris flow. Based on the Xiejiadianzi landslide, Yang et al. (2011) designed a skew test device and discussed the influence of factors such as the instability volume of the source area, the particle size of the test material and the surface roughness of the movement path on the movement distance and speed of the debris flow. In terms of numerical simulations, Chiamin (2011) analyzed the influence of different substrate friction coefficients and bonding strengths on landslide movement accumulation through discrete element calculations Ji et al. (2013) established a numerical model of rock and soil collapse motion by using the PFC3D software and studied the evolution process of particle position movement and velocity in different parts of cohesive and non-cohesive soil during the process of instability development, acceleration and accumulation and conducted a comparative analysis. Zhang et al. (2012) used the PFC3D software to simulate the Jiweishan landslide in Wulong, Chongqing and studied the movement process of the landslide body along the sliding surface under the action of gravity as the dominant sliding force. Sun et al. (2020) proposed a virtual element method strength reduction technique for slope stability analysis, which could be used to study the effects of particle size, rock content, rock density and rock spatial distribution on the mechanical behavior of stony-soil slopes.

In this paper, model tests on non-cohesive spherical granular accumulation were carried out, and the particle movement process and accumulation under the influence of different volume and gradation were analyzed. Using the PFC3D software, a three-dimensional numerical model of particle movement and accumulation was established, and model parameters were calibrated according to the results of the model tests, so as to study further the particle movement and the accumulation at the bottom of the slope.

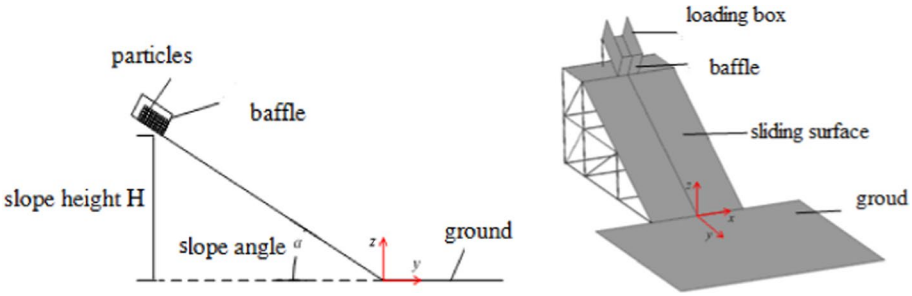

Fig. 1 Sketch of test equipment

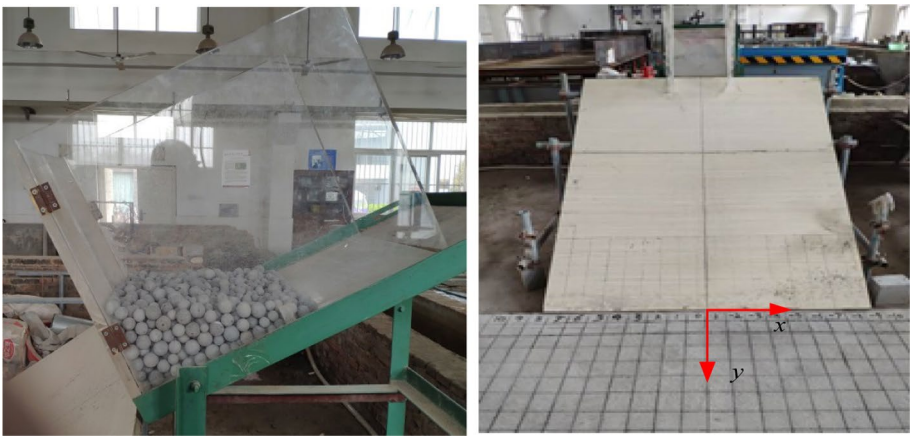

Fig. 2 Physical diagram of test equipment

2 Model tests

2.1 Test equipment and materials

The model device consisted of four parts: the loading box, the sliding surface, the sliding surface support and the slope-bottom accumulation ground plane, respectively. A sketch of the test equipment is shown in Fig. 1. The rectangular coordinate system was established at the bottom of the slope. The size of the loading box was 60 cm × 40 cm × 50 cm (length × width × height), the left- and right-hand sides of the loading box were sealed, while the upper and rear sides were kept open for loading, and a baffle was set in front of the loading box to control the start of the sliding of the entire accumulation body. The sliding surface was composed of smooth wooden boards with a width of 1.8 m on an inclined surface supported by steel-pipe scaffolds, and the height of the slope could be changed by adjusting the scaffolds. At the start of a test, the left- and right-hand side baffles were opened artificially, and the particles in the box could then move downward along the sliding surface under the action of gravity, eventually accumulating on a flat concrete floor. A physical diagram of the test equipment is shown in Fig. 2.

Non-cohesive granular particles were made in-house of C25 cement mortar. To achieve the desired gradation of particles, spherical particles with sizes of 16 mm, 20 mm, 24 mm, 28 mm and 30 mm were produced, as shown in Fig. 3.

2.2 Test program

Because the high-speed and long-distance landslide debris flow occurs under the different topographic and geological conditions, the change of the particle size range, the volume change of the accumulation body and the proportion of the size of the particles also vary. In order to study the influence of the volume and gradation of the accumulation body on the movement and distribution of the particles, accumulation bodies composed of spherical particles of different sizes was selected for the model tests. Considering the impact distance of spherical particles and the specific conditions of the test site, the slope inclination angle of the test model was set to 30°, the slope height (H) at the bottom of the accumulation body was 1.0 m, and the inclination angle of the loading box was consistent with the slope inclination angle.

According to the gradation curve shown in Fig. 4, there are three kinds of grading methods and five types of spherical particles of different sizes. The number of particles of each size required for each group of tests was determined, and each group of tests was repeated six times, such that a total of 30 tests were carried out. The detailed test program is listed in Table 1.

For each group of experiments, the corresponding number of particles was selected and evenly mixed and then placed into the model tank. Then, the surface of the accumulation body was leveled to keep the upper surface even, and the front baffle of the loading box was opened. Under the action of gravity, the accumulation body in the model groove pushed the baffle away automatically, rushed out of the model groove and slid down the slope.

The weight of a single particle was measured by using a spring dynamometer and a rope, and then the maximum static friction force in the critical sliding state was measured by pulling the particles on a horizontal sliding surface. In this way, the coefficient of friction between the particles and the slope surface was measured as 0.42.

Because of the need to analyze the movement and distribution of the accumulation body, after each simulated landslide test, the particles would stop on the ground. In order

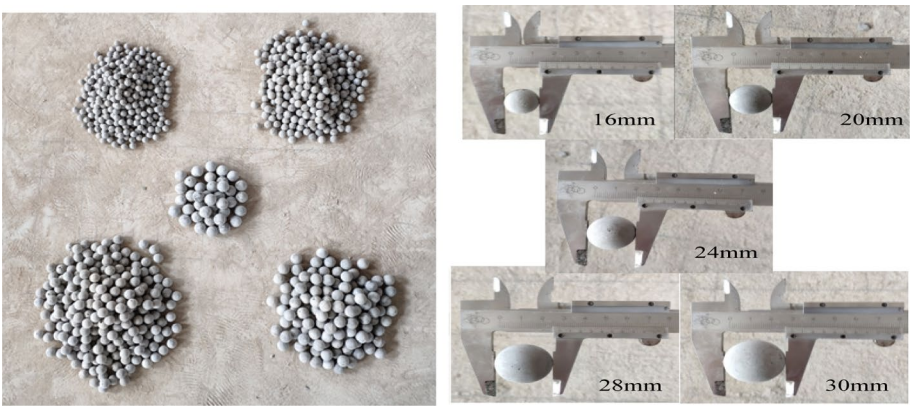

Fig. 3 Photograph of spherical particle

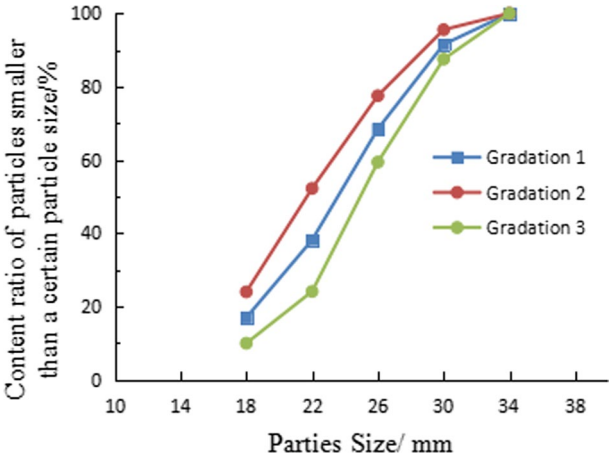

Fig. 4 Gradation curve of test materials

Table 1 Test schemes

Group number	Gradation	Accumulation volume /L	Number of particles					
			16 mm	20 mm	24 mm	28 mm	30 mm	Total
A	Gradation 1	7	223	204	168	81	24	700
B	Gradation 1	11	350	320	265	127	38	1100
C	Gradation 1	15	477	436	361	173	52	1500
D	Gradation 2	11	495	426	221	99	20	1261
E	Gradation 3	11	205	214	309	155	56	939

to observe the distribution range of the final accumulation body and collect the test data conveniently, as shown in Fig. 5, a 10 cm × 10 cm coordinate grid was drawn on the ground with an *x*–*y* coordinate system. A camera was placed at a distance from the bottom of the slope to record the movement of the particles.

3 Analysis of model test results

3.1 Analysis of sliding process of accumulation body

The slip of non-cohesive granular accumulation on the slope surface is apparently different from the ordinary landslide movement. Because the particles were regular spheres, their fluidity was more obvious in the process of movement. After accelerating, the accumulation body mainly moved by rolling on the sliding surface, and a small number of particles jumped.

The particles mostly distributed over a 70 cm × 40 cm (length × width) area, which was divided into many square grids of the same size (10 cm × 10 cm). Marked the grids (1 to 20) from the origin of the coordinates along the positive x-axis. For each test, the total number of all particles was recorded as T, and the total number of particles of each size was recorded as D. Under the different y values, the total number of particles within 0–20

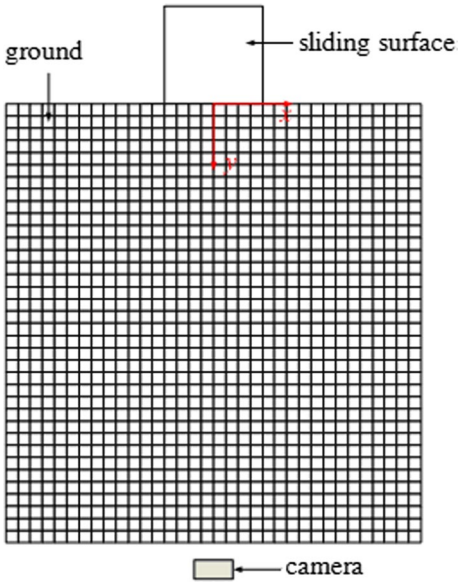

Fig. 5 Diagrammatic sketch of grid division in accumulation area

grid was recorded as T_x, and the number of particles of each size within 0–20 grid was recorded as D_X.

The results of six repeated Group B tests are shown in Fig. 6. The leading edge particles began to move first after the baffle of the loading box was removed. Due to the large height difference of the particles in the upper part relative to the particle size, the particles moved forward in a collapsing way, which hindered the particles in the lower part. After colliding with the slope, there was a significant jump. Because of less obstruction, the velocity of leading edge particles was markedly larger, and a few particles even jumped along the slope. The middle and rear particles had a longer start-up time than the front particles before they began moving due to the interlocking between the particles. During the start-up process, the front particles exhibited obvious lateral expansion, and the edge particles spread to both sides. However, when the lateral expansion reached a certain degree, the front particles stopped expanding to both sides and moved along the direction perpendicular to the foot of the slope. Moreover, after accelerating

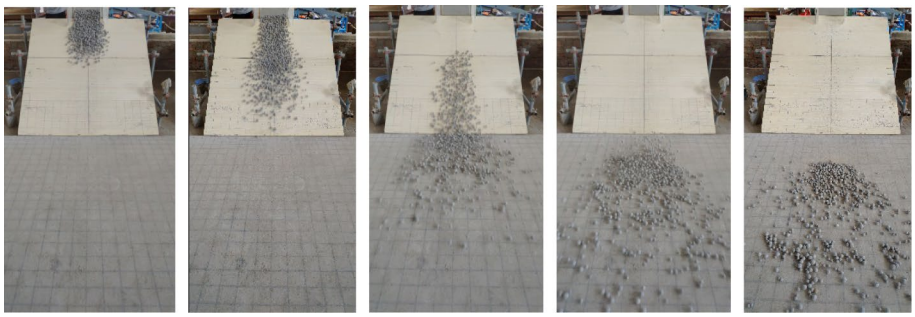

(a) t=0.5s **(b)** t=0.75s **(c)** t=1.3s **(d)** t=1.75s **(e)** t=3s

Fig. 6 Particle motion process

for a certain period, the front end of the particles showed a shuttle-shape, and there was a clear gap between the front and the rear particles. The size of the front end particles was obviously larger, while the velocity of the particles located in the middle part was slightly larger than that at the edge on both sides. It is observed that the particles in the middle part were affected more by the rear particles in the acceleration phase, while the particles in the middle and rear part kept a small angle and moved to the bottom of the slope. After the particles reached the bottom of the slope, they collided with the ground and bounced violently. After bouncing, the front particles continued to expand horizontally and roll forward. The middle and rear particles, after a short bouncing, collided with the front stopping particles, decelerated and started to accumulate. At the same time, there were some particles rolling and expanding to both the left- and right-hand side.

As shown in Fig. 7, in the six tests, within a certain accumulation range, the difference in the proportion of the number of particles was not significant, because the overall accumulation distance of particles largely depends on the movement distance of particles arriving first at the bottom of the slope. However, because the particles in the front end were affected by the presence of the initial accumulation particles and the start-up process, the distribution of the particles stopped at the far end was relatively scattered and not regular.

As shown in Fig. 8, more than 80% of the small size particles, such as 16 mm and 20 mm, were distributed in the 0–20 grid. For particles with a relatively large particle sizes (24 mm and 28 mm), the content of the particles was less than that of the smaller particles in the 0–20 grid, which indicates that the larger the particle size, the smaller the proportion in the close range and the larger the impact distance of the larger particles. Near the end of the accumulation, especially in the 6–10 grid, the 16 mm particles accounted for much more than their proportion in the original accumulation, and the proportion of 20 mm particles was always slightly higher than their original proportion. In the process of particles accumulation, small particles at the end of the accumulation body were found at the back, whereas large particles at the front. The closer to the bottom of the slope, the larger the content of small particles was. With the increase in the accumulation distance, the content of each size particles approached the original proportion.

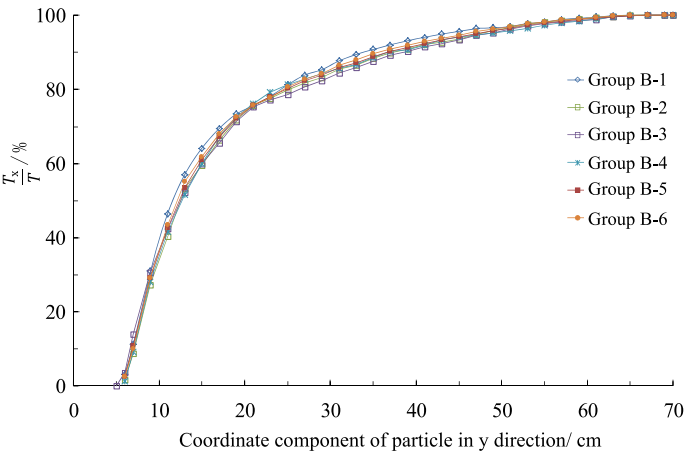

Fig. 7 Proportion of particles within stopping distance

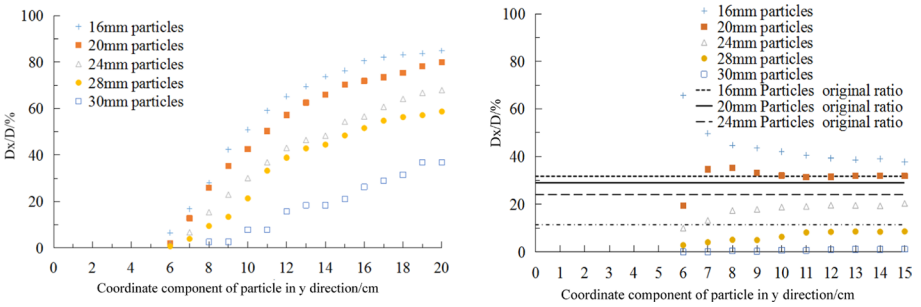

Fig. 8 Distribution of particles with different sizes in 0–20 grid

3.2 Volume effects of accumulations

During the movement of landslide debris flow, the internal effect of sliding body particles was very obvious, and the change in the sliding body volume had far-reaching influence on the particle sliding and accumulation distribution after sliding. Three groups of the same gradation, but different volumes, i.e., Groups A, B, and C, were selected for a comparative analysis. Figure 9 illustrates the start-up and acceleration process on the slope for Groups of A, B and C. Initially, all particles moved forward together, but as the particle velocity increased, it became obvious that the large particles were mainly distributed in the upper part of the body, and the small particles were blocked and sank slowly. With the increase in the volume of the accumulation body, the phenomenon on the surface of the large particles sliding body was more obvious. After a period of acceleration, the shuttle-shape of the

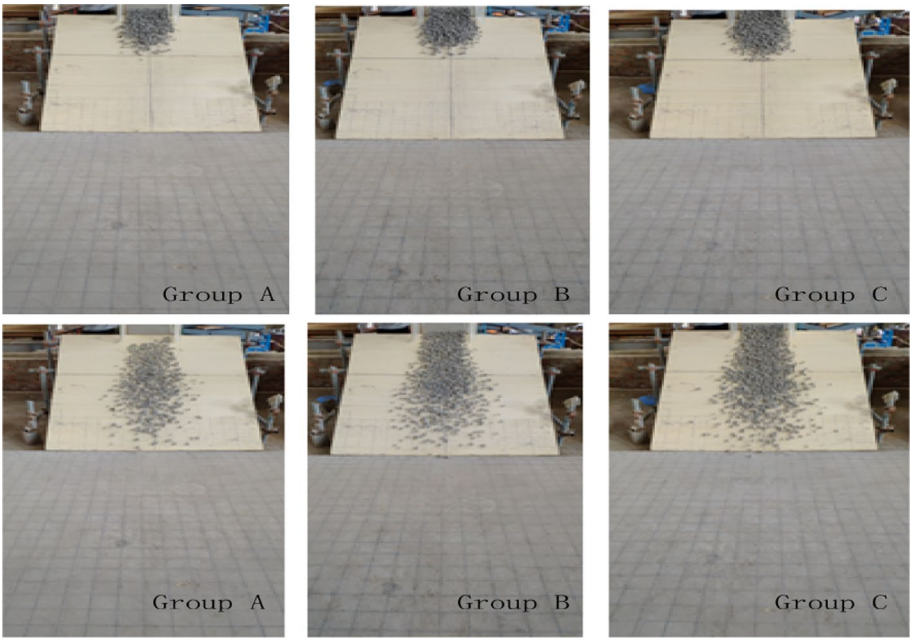

Fig. 9 Accelerated motion process of group A, B and C tests

front-end particles was more obvious, the velocity of the middle-front particles increased and the lateral expansion of the edge part was also larger.

As shown in Fig. 10, as the volume of the granules became larger, the final accumulation of particles also changed significantly. The particles were accumulated farther in Group A than in Groups B and C. It can be seen that the increase in the volume forced the end of the accumulation body closer to the bottom of the slope, but after the volume reached a certain value, the effect was reduced. The increase in volume of the accumulation body led to an increase in the number of rear particles blocked by the front particles during the initial start-up phase, and the acceleration time required for the rear particles was longer; however, the acceleration distance was reduced. As a result, particles achieved a lower speed at the bottom of the slope, the accumulation distance of particles at the end became shorter and the collisions with the particles in front more intense. The subsequent particles reached the bottom of the slope and diffused to both sides after collision, and the distribution range widened.

In the Group C tests, it was obvious that some of the large size particles could not cross the previously arrested small size particles at the beginning and were stack on top of the small size particles. Among the subsequently arriving particles, the large particles could jump over the previously stopped small particles and continued to move forward, eventually depositing in front of the accumulation body and above the small particles, while the small particles were subsequently more decisively blocked at the end of the accumulation body. The particles were more closely distributed at the end of the accumulation body, and the width and the lateral spread of the accumulation body were larger, but the maximum expansion width was less affected by the volume change. For the front-end particles, the difference in impact distance was not large. The main reason is that the front-end particles first achieve a higher velocity after starting, and the collisions with other particles are greatly reduced. Their impact distance largely depends on the slope height and sliding surface properties.

During the movement of the particles, the resistance is not only derived from the friction of the slope surface, but also from the energy loss due to collisions among particles. With the increase in the volume of accumulation body, the intensity of collisions of internal particles increases, especially during stopping at the bottom of the slope, which results in decrease in the stopping distance of particles at the rear of the accumulation body. Due to the small mass of the small size particles, they are easily affected by the large particles during collision and contact and change their motion state and path. During acceleration, the motion of large particles is relatively easy to

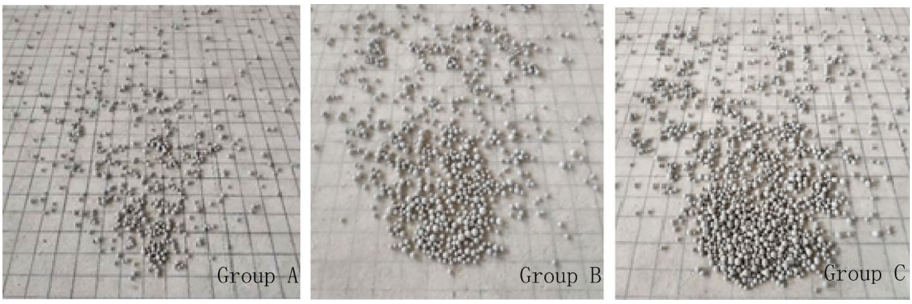

Fig. 10 Particle distribution at end of accumulation body in Groups A, B and C

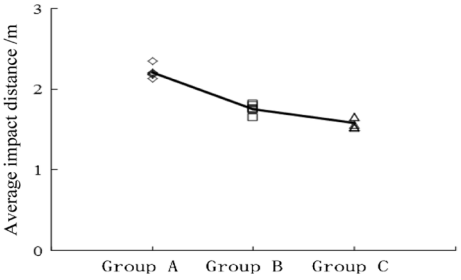

Fig. 11 Comparison of impact distance of accumulation body in each test group

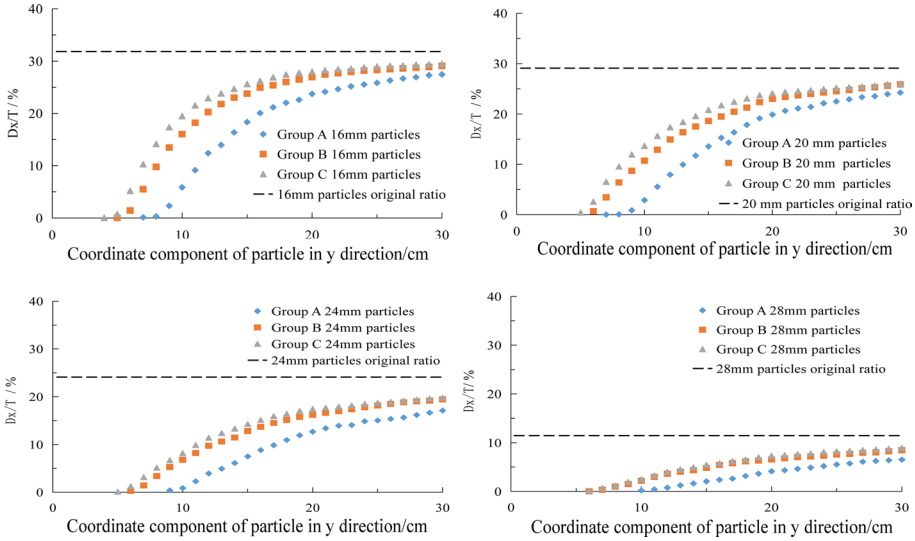

Fig. 12 Proportion of particles with different sizes at different accumulation distances

maintain, and the energy loss is smaller, so it is easier for them to develop velocity and then stop to the front end. When the volume of the accumulation body increases, the accumulation range of the final accumulation body obviously extends, but the accumulation of particles is closer to the bottom of the slope. As shown in Fig. 11, the average impact distance of particles decreased with the increase in the volume of the accumulation body.

As shown in Fig. 12, in the test of three different volumes of accumulation body, i.e., Groups A, B and C, the similar trends developed with the impact distance distribution. The closer the small particles accumulated from the bottom of the slope, the more the particle content per unit impacted the distance. As the stacking distance increased, the number of particles in the unit area was greatly reduced. However, for large particles, such as 28 mm particles, the increase in particle number was approximately linear with the impact distance from the bottom of the slope, and the large particles distributed far beyond the small particles in the distal end of the accumulation body.

3.3 Effect of particle gradation

Three tests of Groups B, D and E were used for comparison, and the volume of particle accumulation was kept constant. The content of small- and medium-sized particles (16 mm and 20 mm) in Group D was the highest, accounting for 50% of the total mass, while the content of small- and medium-sized particles in Group E was the least, accounting for 25% of the total mass, respectively.

As shown in Fig. 13, during the initial particle acceleration phase, the lateral expansion of particles was greatly affected by particle size. The lateral expansion of particles was the largest, and the shuttle-shape of the front particles was more pronounced. The distribution of particles at the edge was thinner than that in the middle part, and the interactions between particles were weaker. From Group D to Group B to Group E, the sparse phenomenon was becoming more obvious with the increase in the proportion of large size particles.

The distribution area of particles at the proximal end of Group D was higher than that of the other two groups, and the particles were more closely spaced. The particle distribution between the middle and the front end of the accumulation zone did not differ significantly. The overall shape was relatively regular, and the maximum width of the lateral expansion of the particles was essentially the same. With the increase in the content of small size particles, the area of particles distribution in the five grids at the end of the accumulation body also increased, and the distribution of small size particles became more concentrated. As shown in Fig. 14, in the three groups of experiments, the increasing trend of the number of 16 mm and 20 mm particles was more consistent, which shows that the velocity did not change much with the increase in impact distance, and the average stopping distance from the bottom of the slope was similar. From Fig. 15, it is obvious that the stopping position of large particles in Group D, such as 24 mm and 28 mm particles, was farther from the bottom of the slope, their proportion at the end of the accumulation body was greatly reduced,

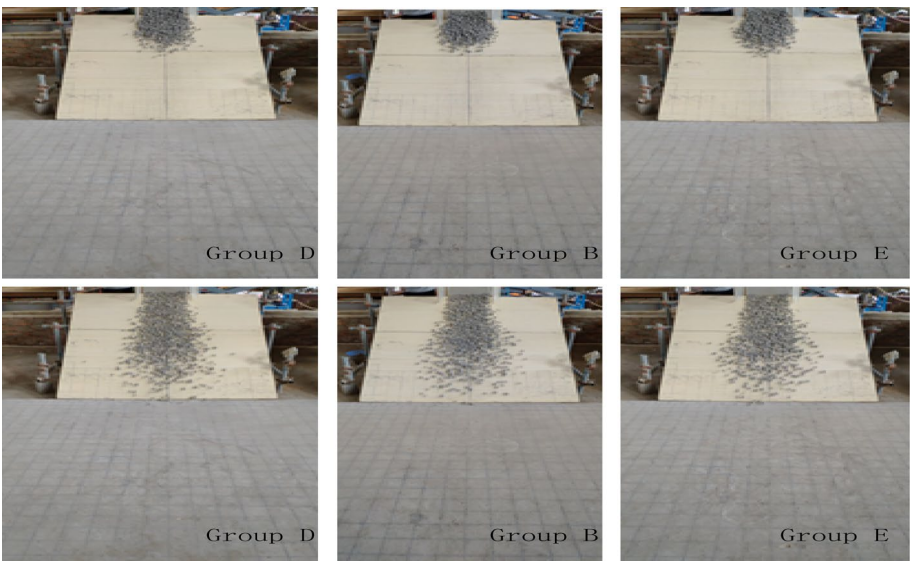

Fig. 13 Accelerated motion process of Groups D, B and E

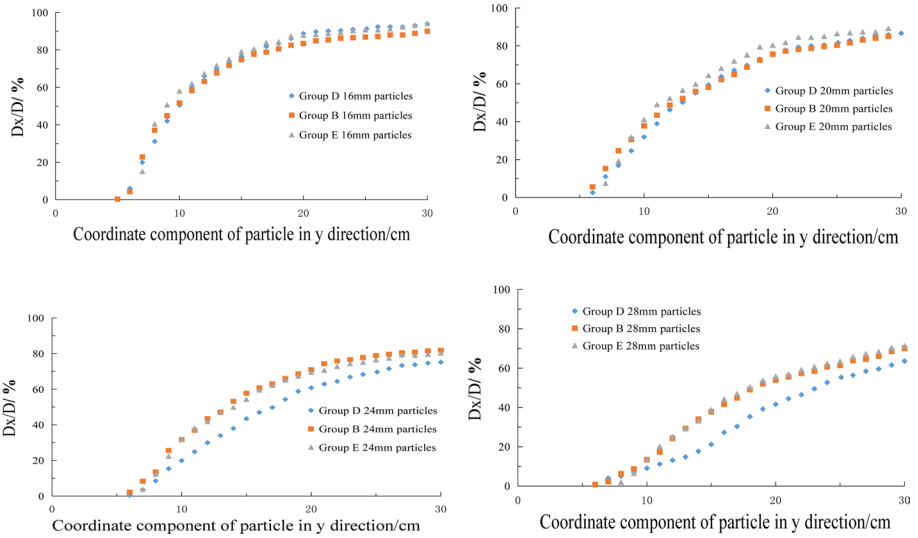

Fig. 14 Proportion of particles within accumulation distance in y-direction

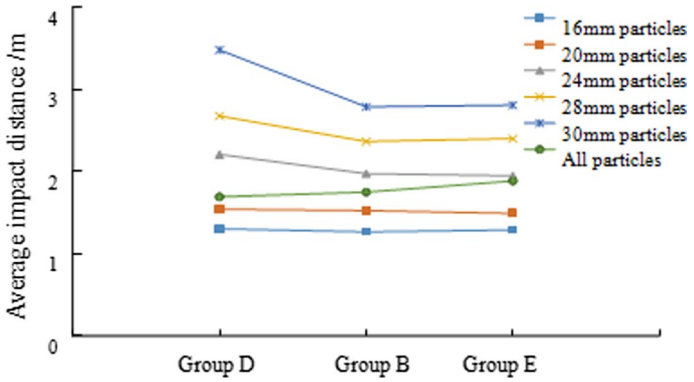

Fig. 15 Comparison of average impact distance of particles of different sizes

and the average stopping distance was farther than that in Groups B and E. The main reason is the increase in the content of small particles and the decrease of large particle content. It is easier for large particles to obtain the energy transferred from small particles to move forward and reach the front end.

4 Numerical simulations

4.1 Modeling

According to the dimensions of the laboratory physical model test device, the loading box, slope surface and slope bottom composed of rigid walls were generated. As shown

in Fig. 16, the slope inclination angle of the whole model was 30°, the slope height at the bottom of the accumulation body was 1.0 m, and the inclination angle of the loading box was consistent with the slope inclination angle. Particle geometry was generated by using the gradation curve and the number of particles in each group in the test program, and the particles of different sizes were grouped.

The particles were spherical in shape and moved mainly in the rolling mode. Therefore, the Rolling Resistance Linear Model (RRLM) was chosen for the contact between particles, as well as between particles and walls. The RRLM was established on the basis of a linear model, to which rolling resistance mechanism was added. After the contact definition was completed, the initial equilibrium of the particle accumulation body was considered. Suspended particles were eliminated after initial equilibrating of the particles, ensuring that each particle kept at least three contact points with the surrounding particles and/or the walls.

4.2 Calibration of parameters

The parameters of the numerical model, such as the stiffness coefficient, friction coefficient, and damping, varied considerably compared to the general macro-parameters. It was, therefore, necessary to compare and back-analyze the laboratory test results to calibrate the specific values of the parameters. Since the rigidity of the particles and the walls have little effect on the movement energy consumption of the particles, which instead is greatly affected by the particle friction coefficient and rotation resistance coefficient, it became important to specify correctly the friction coefficient (μ) and the rotation resistance coefficient (μ_r) in the numerical model. By carrying out a test on the natural angle of repose, and comparing the results of the laboratory model test and the numerical simulation, the friction coefficient (μ) and the rotation resistance coefficient (μ_r) of the RRLM were obtained.

The natural resting angle test on the granular materials was carried out under static pressure and without side walls. As shown in Fig. 17, the detailed steps of the laboratory model test were as follows:

1. A steel cylinder with a diameter of 24 cm and a height of 24 cm was chosen.
2. A total of 1100 particles from Group B were selected, mixed evenly, and then loaded into the cylinder. The particles and cylinder were inverted on the ground.

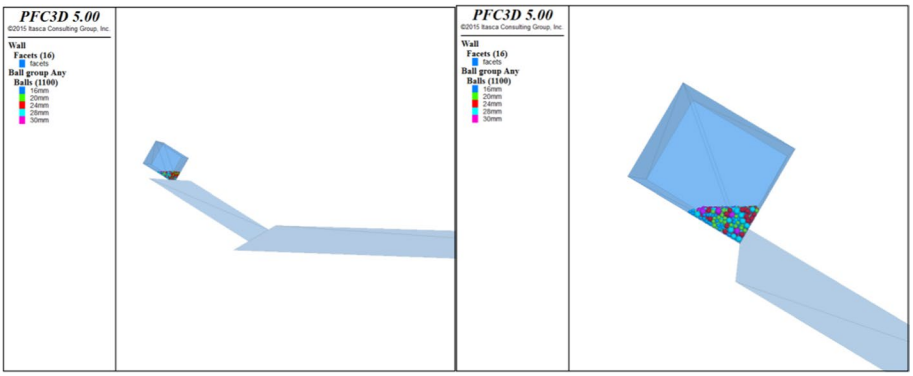

Fig. 16 Model for numerical simulations

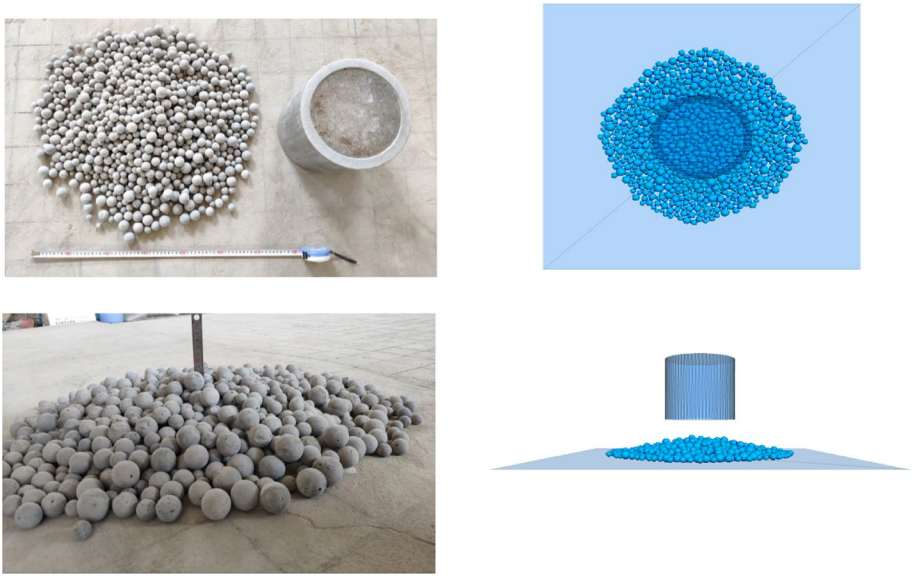

Fig. 17 Comparison of results of natural repose angle test and numerical simulation

3. 3.The cylinder was lifted from the bottom to the top manually at uniform speed, so that the particles could accumulate on the ground surface under the action of gravity.
4. The distribution range of the particles was a circle with a radius of 30 cm, the height of the central part of the accumulation body was 6.7 cm, and the natural angle of repose of the particles was about 24.1°, respectively.

Meanwhile, the same model was established in PFC3D software. The contact model between particles and particles with walls was chosen as RRLM. A cylindrical wall simulation cylinder with a size of 12 cm × 24 cm (radius × height) was established, and 1100 spherical particles were generated according to test Group B specifications. After the model was balanced, the wall was given a certain upward velocity to simulate the same operating conditions as in the laboratory model test. The friction coefficient (μ) and the rolling resistance coefficient (μ_r) were adjusted. When the friction coefficient (μ) was 0.16, and the rolling resistance coefficient (μ_r) was 0.05, respectively, the accumulation range of particles was consistent with the laboratory model test.

Using the determined friction coefficient and damping parameters of the walls, the parameters related to the particles and the walls were selected to run the whole numerical model. The movement process of the particles and the position coordinates of the final particles were recorded, and the accumulation range and impact distance after sliding were analyzed. Compared to the completed laboratory test results, the appropriate parameters were adjusted to make the laboratory tests consistent with the numerical simulation results. The stiffness of walls and particles, and the coefficient of friction among particles are listed in Table 2.

Table 2 The parameters of numerical simulation

Relevant parameters	Parameter value	
Normal stiffness coefficient of wall /(N/m)	*wall_kn*	4×10^6
Tangential stiffness coefficient of wall / (N/m)	*wall_ks*	4×10^6
Normal stiffness coefficient of particles /(N/m)	*clump_kn*	4×10^6
Tangential stiffness coefficient of particles /(N/m)	*clump_ks*	2×10^6
Friction coefficient of wall	*wall_fric*	0.30
Friction coefficient of particles	*ball_fric*	0.16
Rotation resistance coefficient of particles	μ_r	0.05
Damping	βn	0.10
	βs	0.00

5 Analysis of numerical simulation results

5.1 Analysis of particle motion in numerical simulations

Landslide-debris flow movement can generally be conceptualized as two stages, namely, the initial acceleration followed by the deceleration accumulation. In the previous sections, the volume of the accumulation body and particles gradation were controlled in laboratory experiments to compare and analyze the particles distribution and the accumulation. Now, PFC3D numerical simulations are used to study the movement and trajectory of particles.

Taking the numerical simulations of Group B for detailed analysis, the initial acceleration process of particles on the sliding surface was analyzed. As shown in Figs. 18 and 19, the particles began to move downward under the action of gravity after the front door of the loading box was opened. First, the front particles were tipped. Due to the large height difference between the upper particles and the slope, the larger gravity potential energy made them jump and move forward rapidly after contacting the slope surface. For example, large size particles, such as 24 mm and 28 mm, had obvious advantages in the process of tipping collision, and particle acceleration was greater. The

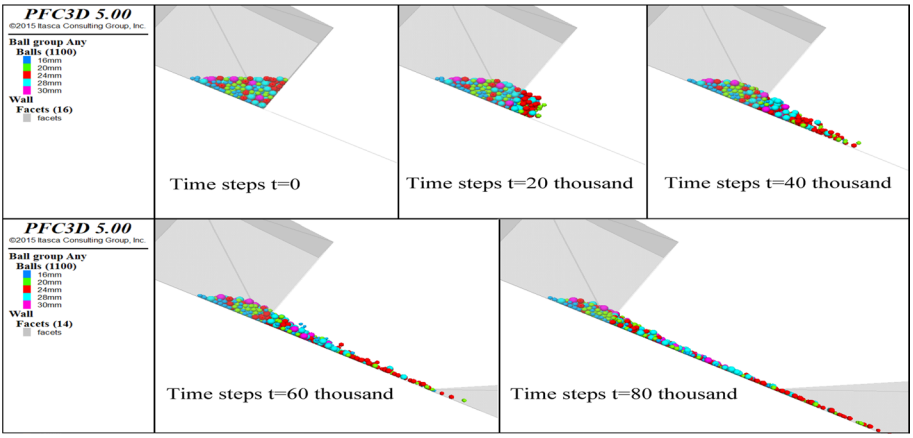

Fig. 18 Numerical simulation of particle motion process

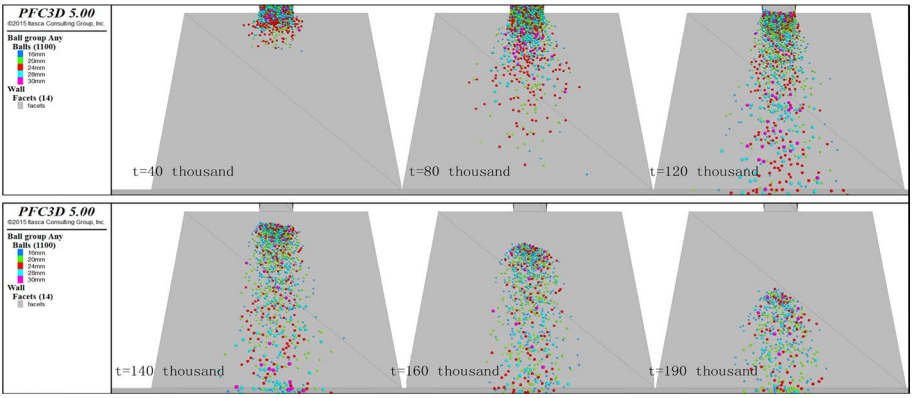

Fig. 19 Front view of particle motion

particles at the edges on both sides could be affected by the particles in the middle part during the overturning process, so there was a very obvious expansion phenomenon. The particles in the middle were affected by the rear particles, and their acceleration was larger than that of the particles scattered on both sides. Thus, their velocities were larger than those of the particles on both sides, which caused all the particles to appear in a shuttle-shape before reaching the slope. The rear particles were slow due to the front particle blocking and internal interactions, and accelerated the movement as the front particles moved away. During the initial acceleration phase, all the rear particles slid forward in clusters. As the particle speed increased, it could be clearly seen that the velocity of particles on both sides was significantly higher than that in the middle, and the rear part of the entire particle volume appeared to be upwardly convex. At the same time, the large particles, initially clustered as a group, separated slowly from the group and moved forward at a faster speed.

Several points of the initial accumulation were selected for analysis. As shown in Fig. 20, considering the symmetry of particle accumulation, 10 points near the edge of the loading box and in the middle were selected. The particles at the edge were denoted

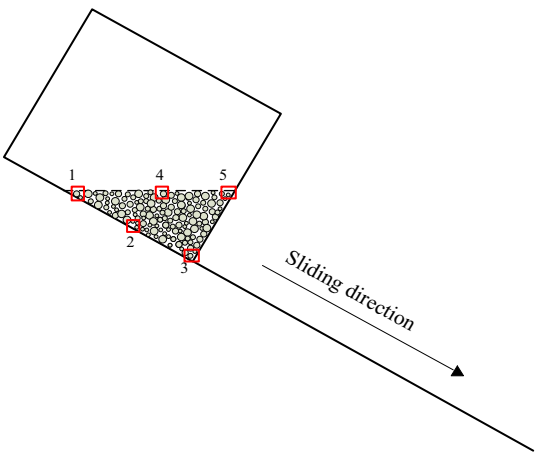

Fig. 20 Particles in selected positions

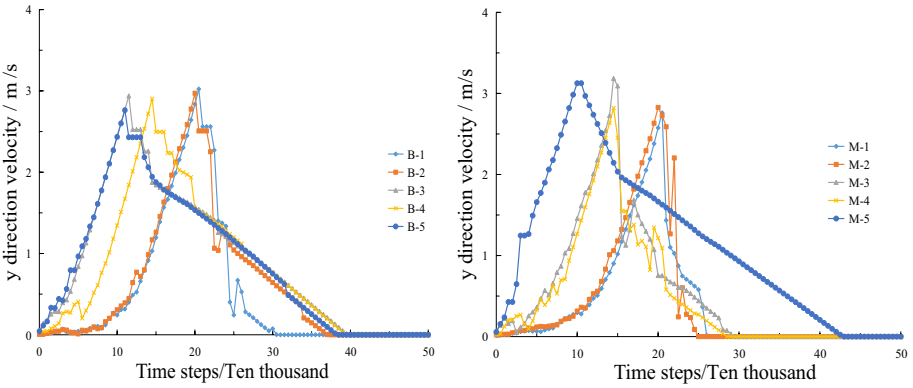

Fig. 21 Velocity of selected particles in *y*-direction versus time

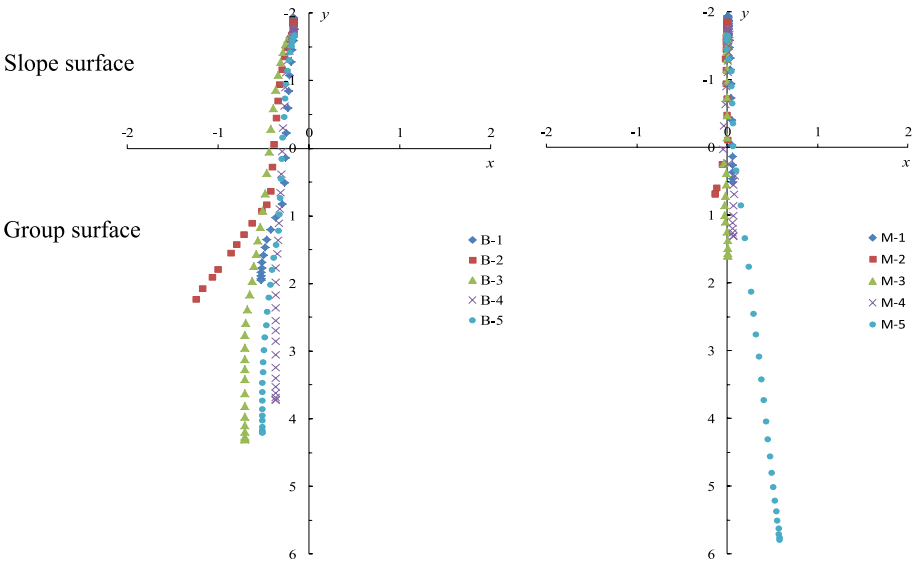

Fig. 22 Motion trajectory diagram of selected particles

as B-1, B-2, B-3, B-4 and B-5, while the particles in the middle as M-1, M-2, M-3, M-4 and M-5, respectively.

Tracking and recording the velocity (y-direction) and position coordinates of marked particles (Fig. 20). The relationship between the sliding velocity and time step is shown in Fig. 21. The position coordinates of particles were projected onto the *x*–*y* plane as shown in Fig. 22. The following observations can be made:

1. For the particles at the upper part of the leading edge (B-5 and M-5), the velocity in the y-direction fluctuated significantly during the start-up acceleration stage, indicating that the particles jumped several times during the start-up overturning process, and the

particles at the edge jump more times than those in the middle. For the particles in the upper part (M-4 and B-4), the velocity in the y-direction decreased significantly after a brief acceleration period, indicating that the particles in the middle collided with the particles in front and were blocked after the acceleration period. The velocity and acceleration of particles in the lower part of the accumulation (B-1, M-1, B-2, and M-2) were both small during the start-up phase. As the front particles moved away, the rear particles started to roll faster.

2. In the start-up phase, the edge particles began to spread to both sides, and the higher the initial position was, the greater the spread angle was. At the same time, from the front to the back of the accumulation body, the horizontal expansion range was getting smaller. The reason for that may be that the particles at the edge collided with the middle particles when they started moving, and the thrust of the particles behind them changed the direction of movement and spread to both sides. The further behind the particle position was, the less the particle was affected by the rear particles, and the diffusion range also became smaller. During the acceleration process on the slope, the particles in the middle (except for M-5) were less disturbed and moved essentially along the center line during the acceleration process, without obvious diffusion.
3. After the particles (especially the rear particles) collided with the front decelerating particles after reaching the bottom of the slope, they continued to expand to both sides of the movement in the x-direction. Due to the obvious expansion of the edge particles during the acceleration stage, the expansion was more obvious at the bottom of the slope, while the spread of particles in the middle part was obviously smaller during the accumulation process at the bottom of the slope.
4. For particles at the same position, such as particles at positions 1 to 4, the impact distance of the particles at the edges was greater than that of the middle particles, mainly because the particles at the edges could deflect to both sides and continue to move forward after colliding and accumulating at the bottom of the slope due to the expansion of the acceleration stage. On the other hand, the particles in the middle were completely blocked by the particles in front of them. For the particles at position 5 (Fig. 20), they were less affected by other particles during acceleration, and the impact distance was the farthest.

5.2 Comparative analysis of numerical simulations and model tests

As shown in Fig. 22, the particle distribution pattern in numerical simulation is consistent with that in the physical test. Due to the collision and blocking effect between the particles, the particles mainly accumulated in the 5–10 grid area and displayed a fan-shaped distribution near the slope bottom. In the process of forward movement, the lateral expansion of particles was limited, and the particles were distributed in a rectangular range, far away from the bottom of the slope.

It can be observed from Fig. 23 that the distance between the particles at the end of the accumulation body obtained in the physical model tests is consistent with the numerical simulations. Large particles mainly stopped at the far end, while small particles mostly accumulated at the near end. However, the near-end particles were more evenly distributed in the numerical results. In the numerical simulations, there were also many particles at the far end. It can be seen that the calculation of energy exchange loss in the process of particle

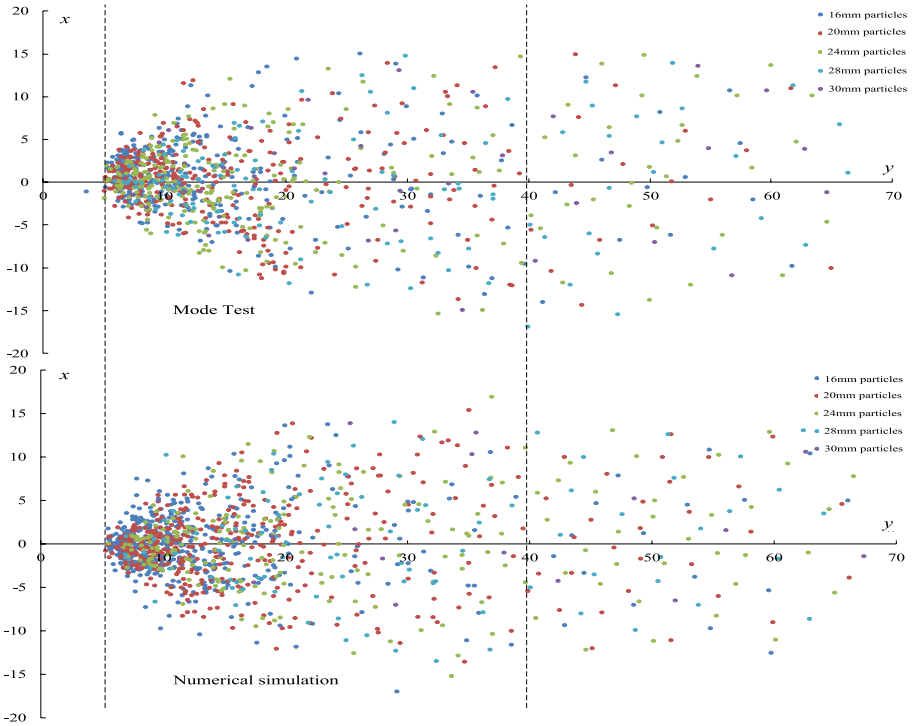

Fig. 23 Accumulation and distribution of particles with different sizes in tests and numerical simulations

collision was simplified and could not fully simulate the interactions between particles. Figure 24 shows the average stopping distance of particles with different sizes. The average stroke of particles with small size was relatively consistent. The stopping distance of large particles was far beyond that of small particles, which indicates that large particles can more easily obtain energy and maintain their motion, while small particles are easily

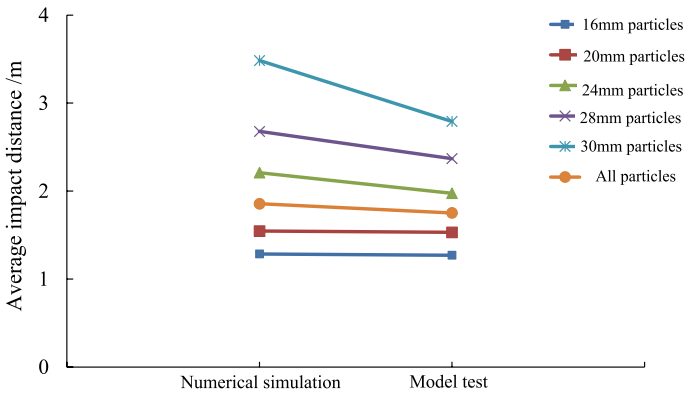

Fig. 24 Comparison of particle impact distance between numerical simulations and model tests

affected and obstructed by other particles, and so their stopping distance was shorter. Comparing the results of numerical simulations and physical model tests, the particle accumulation distribution and movement process have the same regularity, which shows the reliability of the discrete element method simulations.

6 Conclusions

1. The sliding accumulation of spherical granules shows an obvious reverse pattern of small size particles at the rear and large size particles at the front. With the increase in the volume of the accumulation body, the phenomenon becomes more obvious, and a trend of large particles accumulating above small particles begins to appear.
2. During the acceleration of particles on the slope surface, there is an obvious lateral expansion. The particles keep sliding at a certain angle until they reach the bottom of the slope. In the front part of the particle volume, the "shuttle" phenomenon occurs, because the particles in the middle part are obviously larger than those on both sides, and this phenomenon becomes more obvious with the increase in the content of large particles.
3. The distance between the end position of a particle and the bottom of the slope depends largely on the movement distance of the particles arriving at the bottom of the slope first. Among the subsequent particles arriving at the bottom of the slope, some of the larger particles can jump over the previously stopped small particles and continue to move forward, and stop in the front or above small particles, while the small particles are more blocked at the end of the accumulation.
4. The distribution of particles at the end of final accumulation body is greatly affected by volume, but the larger the volume, the lesser the effect. Also, the stopping distance at the front is less affected by the volume and particle gradation.

In the experiment, a wooden board was used to simulate the slope surface, without considering the impact and wrapping effect of the sliding body on the particles of the sliding surface. At the same time, the selection of the particles of the accumulation body was greatly simplified, without considering the internal structure of the accumulation body, which differs from the actual situations, but from the perspective of understanding the principles of motion, this study can serve as a useful reference.

Acknowledgements This research was supported by National Natural Science Foundation of China (51179043).

References

Chiaming L, Minglang L, Chaolung T et al (2011) A kinematic model of the Hsiaolin landslide calibrated to the morphology of the landslide deposit. Eng Geol 123(1):22–39

He S-M, Bai X-Q, Ouyang C-J, Wang D-P (2017) On the survey of giant landslide at Xinmo village of Diexi Town, Maoxian Country, Sichuan Province. China Mount Res 35(04):598–603

Huang H-Q, Zhao Q-H (2010) Basic characteristics and preliminary mechanism analysis of large scale rockslide-sturzstrom at Wenjiagou triggered by Wenchuan earthquakes. J Eng Geol 18(02):168–177

Hutter K, Koch T (1991) Motion of a granular avalanche in an exponentially curved chute: experiments and theoretical predictions. Philos Trans R Soc Lond Ser A 334(1633):93–138

Ji X-J, Ou G-Q, Yang S, Wang J, Lu G-H (2013) Comparison analysis of the motion process about viscous and no-viscous landslip-collapse soil based on PFC3D. J Sichuan Univ (Eng Sci Edn) 45(S1):67–73
Manzella I, Labiouse V (2008) Qualitative analysis of rock avalanches propagation by means of physical modelling of non-constrained gravel flows. Rock Mech Rock Eng 41(1):133–151
Ma Y, Wu Y-F (2011) "8·13" Extra large debris flow disaster in Wenjia gully of Qingping Township, Mianzhu, Sichuan Province. Chin J Geol Hazard Control 22(01):21
Pudasaini SP, Hsiau SS, Wang Y, Hutter K (2005) Velocity measurements in dry granular avalanches using particle image velocimetry technique and comparison with theoretical predictions. Phys Fluids 17(9):093301
Ren J-W, Shan X-J, Shen J, Sang Ge, Sang Z, Deng G-Y et al (2001) The geomorphology and kinematics of the Yigong collapse-landslide-debris flow in Tibet. Geol Rev 06:642–647
Sun G-H, Lin S, Zheng H, Tan Y-Z, Tan S (2020) The virtual element method strength reduction technique for the stability analysis of stony soil slopes. Comput Geotech 119:103349
Xu Q, Li W-L, Dong X-J, Xiao X-X, Fan X-M, Pei X-J (2017) The Xinmocun landslide on june 24, 2017 in Maoxian, Sichuan: characteristics and failure mechanism. Chin J Rock Mechan Eng 36(11):2612–2628
Yang Q-Q, Fei C, Ugai K, Yamada M (2011) Some factors affecting the frontal velocity of rapid dry granular flows in a large flume. Eng Geol 122(3/4):249–260
Zhang L, Tang H-M, Xiong C-R, Huang L, Zou Z-X (2012) Movement process simulation of high-speed long-distance Jiweishan landslide with PFC3D. Chin J Rock Mechan Eng 31(S1):2601–2611